GPS Solutions (2019) 23:120
https://doi.org/10.1007/s10291-019-0909-0

ORIGINAL ARTICLE

Field of coherence of GPS-measured earth tremors

Alexey Lyubushin[1]

Received: 15 July 2019 / Accepted: 26 August 2019

Abstract
A new method for investigating the coherence field of the noise component of high-frequency GPS time series is proposed. The method is applied to the main territory of the USA, which is characterized by a dense network of GPS stations. The data are presented in steps of 5 min from February 28, 2013, until June 29, 2019, on the Nevada Geodetic Laboratory Web site. The proposed method estimates the spatial distribution of the mean values of multiple coherence, calculated within nodes of a regular grid, between GPS coordinates of a given number of nearest operable stations and the periods at which the maximum values of coherence are reached. The two-dimensional probability density of the positions of places where the coherence maximum is most often realized is estimated. These estimates can be obtained for the entire history of observations and also in a sliding time window of a given length, which makes it possible to trace the dynamics of changes in time in the coherence field of the earth's tremor. The entropy of the two-dimensional probability density of places of concentration of maximum values of coherence allows us to distinguish seasonal changes in the structure of the coherence field of GPS noise. To study the temporal dynamics, we use the auxiliary time series of changes in the maximum multiple coherence at 50 reference points located throughout the study area. The study of the coherence properties of this auxiliary 50-dimensional time series ("secondary coherence") in a 180-day sliding time window highlighted a series of synchronization bursts of earth's surface tremors.

Keywords GPS noise · Spectral coherence measure · Synchronization · Vector autoregression · Entropy

Introduction

Analysis of the fine spectral structure and models of noise component of GPS time series is a traditional object of research. Langbein and Johnson (1997) analyzed spectral indices by fitting the power laws to spectra and estimating their parameters using the maximum likelihood method. The effect of the flicker noise component of GPS time series on velocity errors, including their latitudinal dependence, was investigated in Zhang et al. (1997) and in Mao et al. (1999). Further development of the use of the maximum likelihood method for estimating the amplitudes of white and color (power) noise in GPS time series for various regions is presented in Williams et al. (2004), Bos et al. (2008) and Wang et al. (2012). The task of estimating velocity uncertainty as a function of the magnitude of the spectral index was considered in Caporali (2003). In Li et al. (2000), parametric models of GPS time series were used to identify data breaks characteristic of tectonically active areas. High-frequency GPS noise for a number of areas in New Zealand and the USA has been researched in Beavan (2005) and Langbein (2008). The influence of the seasonal hydrological load on the earth's surface on the determination of the velocities of movement of tectonic plates was studied in Blewitt and Lavallee (2002) and Bos et al. (2010). Teferle et al. (2008) and Chen et al. (2013) used the principal component method to implement empirical orthogonal functions and singular spectrum analysis to highlight common spatial characteristics and seasonal variations of GPS time series. Seismic records of a network of accelerometers were analyzed together with the high-frequency components of the GPS time series in Bock et al. (2011). Hackl et al. (2013) investigated the relationship between the appearance of non-stationary effects in GPS time series and the processes of slow slips at the boundaries between the blocks of the earth's crust. Applications of discrete wavelet transforms to study the properties of GPS time series and to assess station positioning stability

✉ Alexey Lyubushin
lyubushin@yandex.ru

[1] Institute of Physics of the Earth, Russian Academy of Sciences, Moscow, Russia

Published online: 27 September 2019

were considered in Goudarzi et al. (2013) and Khelif et al. (2013). An analysis of the coherence of high-frequency earth's tremor, measured by GPS, to detect the global synchronization effect was used in Lyubushin (2018b). In the works Filatov and Lyubushin (2017, 2019), the analysis of the fractal characteristics of high-frequency GPS time series was used to extract potentially dangerous seismically active regions in Japan and California.

We propose a method for studying the coherence field of the noise component of high-frequency GPS time series based on the use of a vector autoregression model. The main territory of the USA, which is characterized by a dense network of GPS stations, has been taken as the area of application. The proposed method estimates the spatial distribution of the mean values of multiple coherence and the periods at which the maximum values of coherence are reached. In addition, a two-dimensional probability density is estimated for the positions of the places where the coherence maximum is most often realized. These estimates could be obtained both for the entire history of observations and in a sliding time window of a given length, which makes it possible to trace the dynamics of changes in time in the coherence field of the earth's tremors. Estimation of the entropy of the two-dimensional probability density of the locations of the concentration of maximum values of coherence allows us to identify seasonal changes in the structure of the coherence field of the GPS noise. To study the temporal dynamics, the auxiliary time series of changes in the maximum of multiple coherence at 50 reference points spread throughout the study area were constructed. The study of the coherence properties of this auxiliary 50-dimensional time series ("coherence of coherence" or "secondary coherence") in a 180-day sliding time window highlighted a series of ground tremor synchronization bursts.

Data

We used data from the network of 6026 GPS stations which cover the main territory of the USA (longitudes from −127° up to − 65°, latitudes from 30° up to 50°) for the time interval from February 28, 2013, until June 29, 2019. These data present three-coordinate time series of earth's displacements with sampling time step 5 min and coordinates of the stations, and they are available from the Nevada Geodetic Laboratory Web site by address ftp://gneiss.nbmg.unr.edu/rapids_5min/kenv/. The complete data set covers the whole world, and their structure is described in detail in Blewitt et al. (2018).

Figure 1 presents positions of GPS stations and its splitting into 50 clusters by Voronoi polygons with centers of clusters presented by red circles. Positions of the cluster centers (reference points) were found by *k*-means clustering procedure (Duda et al. 2000).

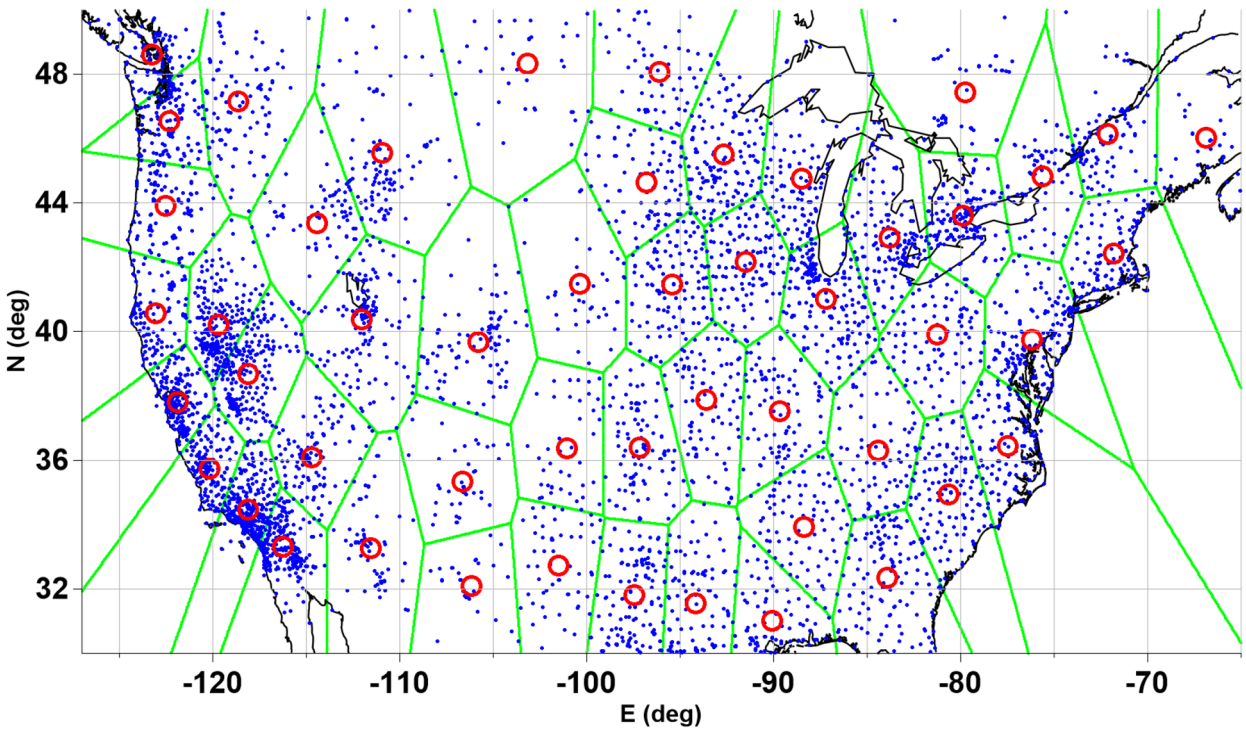

Fig. 1 Network of 6026 GPS stations (blue points) and positions of 50 reference points (red circles). Green lines present Voronoi polygons

Multiple coherence measure

The main tools for GPS time series processing used are multiple coherence measures, which are described in this section. Canonical coherences are the generalization of the usually used squared coherence spectrum between two scalar time series for the case when two vector time series are considered: m-dimensional time series $X(t)$ and n-dimensional time series $Y(t)$. Here t is an integer time index. Without loss of generality, let us suppose that $m \le n$. The squared maximum canonical coherence $\mu^2(\omega)$ between multiple time series $X(t)$ and $Y(t)$ is computed as maximum eigenvalue of the following frequency-dependent matrix (Brillinger 1975; Hannan 1970):

$$U(\omega) = S_{xx}^{-1} S_{xy} S_{yy}^{-1} S_{yx} \tag{1}$$

Here ω is the frequency, $S_{xx}(\omega)$ is the spectral matrix of size $m \times m$ of time series $X(t)$, $S_{xy}(\omega)$ is the cross-spectrum matrix of the size $m \times n$ between time series $X(t)$ and $Y(t)$, $S_{yx}(\omega) = S_{xy}^H(\omega)$, "$H$" is the sign of Hermitian conjunctions (i.e., transposition of the matrix and complex conjugation), and $S_{yy}(\omega)$ is the spectral matrix of size $n \times n$ of time series $Y(t)$. If we take $X(t)$ as scalar i-th component of the q-dimensional time series $Z(t)$, and $Y(t)$ as $(q-1)$-dimensional time series composed of all other scalar components of $Z(t)$, then function (1) becomes scalar which could be called component canonical coherence $v_i^2(\omega)$.

The value $v_i^2(\omega)$ is the measure of connection of variations of the i-th component of the q-dimensional time series $Z(t)$ with variations of all other scalar components of $Z(t)$ at the frequency ω. The inequality $0 \le |v_i(\omega)| \le 1$ is fulfilled, and the closer the value of $|v_i(\omega)|$ to unity, the stronger the linear relation of variations at the frequency ω of the i-th scalar series to analogous variations in all other series. Now we can define the multiple (i.e., multidimensional with dimensionality q) spectral coherence measure by:

$$\lambda(\omega) = \left(\prod_{i=1}^{q} |v_i(\omega)| \right)^{1/q} \tag{2}$$

The value of (2) provides a frequency-dependent measure of linear joint synchronization of variations of all scalar components of time series $Z(t)$ at the frequency ω. Because the dimensionality of series $X(t)$ in (1) equals 1, the matrix $U(\omega)$ in fact is a scalar. Thus, its "maximum eigenvalue" is the value of the following quadratic form divided by the power spectrum of i-th component:

$$v_i^2(\omega) = S_i^H(\omega)(S_{ZZ}^{(i)}(\omega))^{-1} S_i(\omega) \Big/ P_i(\omega) \tag{3}$$

Here $S_{ZZ}^{(i)}(\omega)$ is a Hermitian matrix of the size $(q-1) \times (q-1)$, which is obtained from the full spectral matrix $S_{ZZ}(\omega)$ of the size $q \times q$ of multiple time series $Z(t)$ by removing its i-th column and i-th row; thus, $S_i(\omega)$ is a $(q-1)$ -dimensional vector consisting of the cross-spectrums between i-th component of $Z(t)$ with all its other scalar components. It is evident that vector $S_i(\omega)$ is composed of elements of the spectral matrix $S_{ZZ}(\omega)$ from i-th column except for the elements in the i-th row. Finally $P_i(\omega)$ is a power spectrum of i-th component of $Z(t)$, i.e., the i-th element on the main diagonal of the matrix $S_{ZZ}(\omega)$. The matrix $S_{ZZ}^{(i)}(\omega)$ is Hermitian and positive definite defined—that is why the quadratic form $S_i^H(\omega)(S_{ZZ}^{(i)}(\omega))^{-1} S_i(\omega)$ is real and positive.

For calculating the measure (2) using values (3), it is necessary to estimate the spectral matrix $S_{zz}(\omega)$ of the size $q \times q$. For this purpose, we use the vector autoregression model (Marple 1987; Hamilton 1994; Box et al. 2015):

$$Z(t) + \sum_{k=1}^{p} A_k \cdot Z(t-k) = e(t) \tag{4}$$

where p is an autoregression order, A_k are matrices of autoregression coefficients of the size $q \times q$, $e(t)$ is q-dimensional residual signal with zero mean and covariance matrix $\Phi = M\{e(t)e^T(t)\}$ of the size $q \times q$. Matrices A_k and Φ are defined using Durbin–Levinson procedure, and the spectral matrix is calculated using:

$$S_{ZZ}(\omega) = \Psi^{-1}(\omega) \cdot \Phi \cdot \Psi^{-H}(\omega), \ \Psi(\omega) = I + \sum_{k=1}^{p} A_k e^{-i\omega k} \tag{5}$$

where I is a unit matrix of the size $q \times q$. When $q = 2$, the value (2) equals to usual coherence spectrum:

$$\lambda(\omega) = |S_{12}(\omega)| \Big/ \sqrt{S_{11}(\omega) \cdot S_{22}(\omega)} \tag{6}$$

where $S_{11}(\omega)$ and $S_{22}(\omega)$ are diagonal elements of the matrix (5), i.e., parametric estimates of the power spectra of two signals, and $S_{12}(\omega)$ is their mutual cross-spectrum.

The multiple coherence measure (2) was proposed in Lyubushin (1998) and was applied for seeking earthquakes precursors and investigating low-frequency seismic noise properties Lyubushin (1999, 2014, 2018a). In Filatov and Lyubushin (2019), this measure in combination with fractal analysis of GPS time series was used for detecting seismically dangerous regions in California. In Lyubushin (2018b), the vector autoregression model (4) was applied for extracting effects of global synchronization of GPS-measured earth tremors by processing daily time series from 1191 GPS stations all over the world for time interval 2006–2018.

Estimates of multiple coherence measures for GPS time series

The region which is presented in Fig. 1 is covered by a regular grid of nodes with 125 nodes in longitude axis and 50 nodes in the latitude axis. The observations were split into adjacent time intervals of the length 5 days, i.e., 1440 samples with time step 5 min. Within each time interval and for each node of the grid, the 10 nearest operable GPS are found. The GPS station is considered operable within the time interval if the general number of gaps inside this interval is less than 10% of the interval length, i.e., less than 144 samples. The gaps are filled up by "likelihood" values which are defined using true values from the right and left vicinities of the gap of the same length as the gap length similar to the method which was used in Lyubushin (2018). Furthermore, the trend is removed from the records inside the interval by a polynomial of the 4th order. Thus, the high-frequency components of GPS time series are investigated only.

The vector autoregression model (4) was identified for each node for each time interval for the $q = 10$ nearest operable stations for GPS components E, N and Up separately. We used the 10-dimensional vector AR-model of the fifth order, $p = 5$. Figure 2 presents graphs of several examples of multiple coherence functions (2) for the vertical component Up.

Let us denote by $\lambda_{ij}^{(t)}(\omega)$ the multiple coherence function corresponding to the grid node (i,j) and to the time interval of the length 5 days with number t. Let us consider the following values:

$$\mu_{ij}^{(t)} = \max_{\omega} \lambda_{ij}^{(t)}(\omega), \quad \Omega_{ij}^{(t)} = \arg\max_{\omega} \lambda_{ij}^{(t)}(\omega), \quad T_{ij}^{(t)} = 2\pi/\Omega_{ij}^{(t)} \tag{7}$$

Thus, $\mu_{ij}^{(t)}$ is the maximum values of coherence measure with respect to all frequencies, $T_{ij}^{(t)}$ is period corresponding to this maximum, t is integer index that numerates successive adjacent time windows of the length 5 days. Each grid vector $\mu_{ij}^{(t)}$ and $l_{ij}^{(t)} = \lg(T_{ij}^{(t)})$ could be regarded as "elementary" map of the length 5 days. We can consider averaged maps:

$$\bar{\mu}_{ij}(t_0,t_1) = \sum_{t=t_0}^{t_1} \mu_{ij}^{(t)}/(t_1 - t_0 + 1), \quad \bar{l}_{ij}(t_0,t_1) = \sum_{t=t_0}^{t_1} \lg(T_{ij}^{(t)})/(t_1 - t_0 + 1) \tag{8}$$

which corresponds to some intervals of time index t from minimum t_0 up to maximum t_1. Figure 3 presents the averaged maps (8) for all available time indexes t covering all history of observations 2013–2019 for three GPS components E, N and Up. Let us denote by $\bar{\mu}_{ij}^{(E)}$, $\bar{\mu}_{ij}^{(N)}$, $\bar{\mu}_{ij}^{(U)}$ and $\bar{l}_{ij}^{(E)}$, $\bar{l}_{ij}^{(N)}$, $\bar{l}_{ij}^{(U)}$ the averaged maps (8) for GPS components E, N and Up correspondingly.

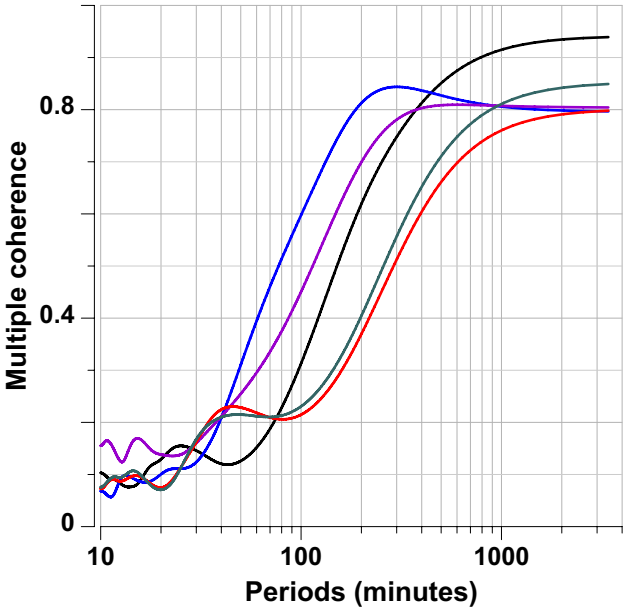

Fig. 2 Examples of five multiple coherence functions for component Up from the 10 nearest operable GPS stations, estimated for different time windows of length 5 days (1440 samples with time step 5 min). Colors of graphics correspond to different cases of coherence functions estimates, i.e., different time windows and nodes of regular grid. This figure illustrates different types of coherence functions behavior and the choice of maximum value of coherence and corresponding period's values. Multiple coherence is a dimensionless value which could vary from 0 up to 1

From Fig. 3, we can notice that maps for horizontal GPS components E and N are rather similar to each other whereas vertical component differs from horizontal ones more significantly. Table 1 contains the values of correlation coefficients between different averaged maps.

Trying to extract common spatial features of maps for different GPS components, we used the weighted mean maps which are calculated according to:

$$\bar{\mu}_{ij}^{(WM)} = \alpha_E^2 \bar{\mu}_{ij}^{(E)} + \alpha_N^2 \bar{\mu}_{ij}^{(N)} + \alpha_U^2 \bar{\mu}_{ij}^{(U)}, \quad \bar{l}_{ij}^{(WM)} = \beta_E^2 \bar{l}_{ij}^{(E)} + \beta_N^2 \bar{l}_{ij}^{(N)} + \beta_U^2 \bar{l}_{ij}^{(U)} \tag{9}$$

Here $(\alpha_E, \alpha_N, \alpha_U)$ and $(\beta_E, \beta_N, \beta_U)$ are eigenvectors of covariation matrices of the size 3×3 of grid vectors $(\bar{\mu}_{ij}^{(E)}, \bar{\mu}_{ij}^{(N)}, \bar{\mu}_{ij}^{(U)})$ and $(\bar{l}_{ij}^{(E)}, \bar{l}_{ij}^{(N)}, \bar{l}_{ij}^{(U)})$ corresponding to their maximum eigenvalues. Equation (9) could be regarded as a variant of the principal component approach (Jolliffe 1986). It should be noted that $\alpha_E^2 + \alpha_N^2 + \alpha_U^2 = 1$ and $\beta_E^2 + \beta_N^2 + \beta_U^2 = 1$. For our case, $\alpha_E^2 = 0.288$, $\alpha_N^2 = 0.308$ and $\alpha_U^2 = 0.404$; $\beta_E^2 = 0.337$, $\beta_N^2 = 0.338$ and $\beta_U^2 = 0.325$.

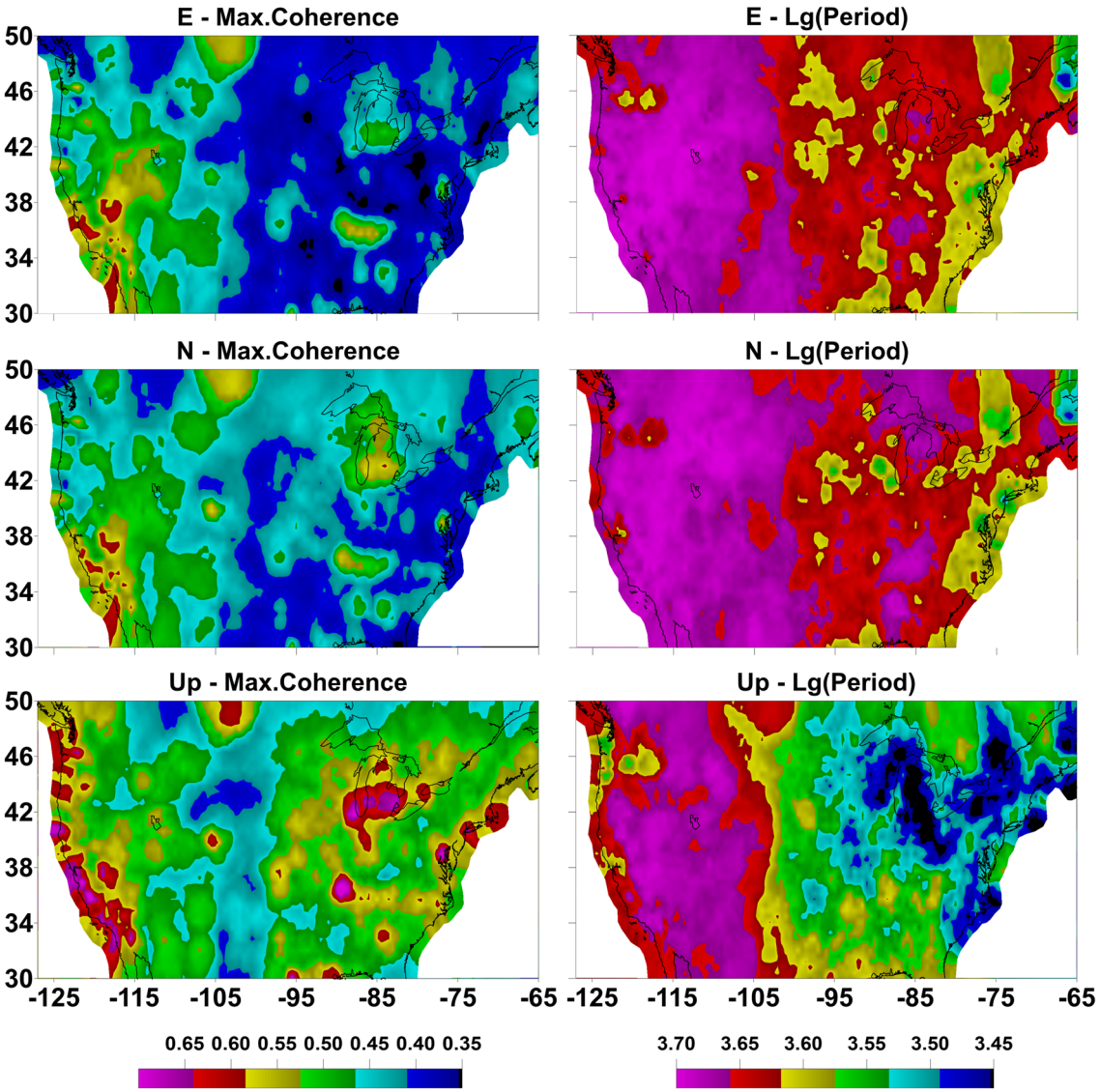

Fig. 3 Figure presents averaged maps of multiple coherence values which were calculated for each node of the regular grid of the size 50×125 from 10 nearest operable stations within adjacent time windows of the length 5 days for the whole interval of observations. Left column presents averaged maps of maximum multiple coherence values for components E, N and Up. Right column presents averaged maps of decimal logarithm of periods (in minutes) which correspond to the maximum of multiple coherence values for components E, N and Up. Maps in the left and right panels have the same color scales, respectively, which are placed below each panel

Table 1 Coefficients of correlation between different averaged maps

	$\bar{\mu}_{ij}^{(E)}$	$\bar{\mu}_{ij}^{(N)}$	$\bar{\mu}_{ij}^{(U)}$
$\bar{\mu}_{ij}^{(E)}$	1	0.9224	0.5499
$\bar{\mu}_{ij}^{(N)}$	0.9224	1	0.5958
$\bar{\mu}_{ij}^{(U)}$	0.5499	0.5958	1
	$\bar{l}_{ij}^{(E)}$	$\bar{l}_{ij}^{(N)}$	$\bar{l}_{ij}^{(U)}$
$\bar{l}_{ij}^{(E)}$	1	0.8241	0.7172
$\bar{l}_{ij}^{(N)}$	0.8241	1	0.7199
$\bar{l}_{ij}^{(U)}$	0.7172	0.7199	1

Figures 3 and 4 show that the field of average maximum multiple coherences forms a distinctly spotted structure with compact areas of increased coherence of earth tremors. We assume that these "coherence spots" arose due to special conditions in the upper part of the earth's crust, which are caused by both the seismic regime and industrial impact, in particular, shale gas production. Considering the averaged maps of the distribution of the logarithms of the periods in which the maximum values of multiple coherence are reached, we can notice that for them the division of the studied territory of the USA into two approximately equal parts is obvious: the West part with high values of the periods and

the East part with lower values of periods. It can be assumed that this difference in the dominant periods of GPS noise coherence mainly is related to the climatic differences of these two parts. It should be noticed that vertical boundary between these two parts (approximately for longitude − 100°) is characterized by lower values of averaged maximum coherences $\bar{\mu}_{ij}^{(U)}$ and $\bar{\mu}_{ij}^{(WM)}$ than for left and right sides from this boundary.

Probability distribution functions of nodes with a maximum of coherence

Let us consider maximum values of coherence as a function of longitudes and latitudes (x_i, y_j) of nodes (i, j) explicitly: $\mu_{ij}^{(t)} \equiv \mu^{(t)}(x_i, y_j)$. For each 5-day "elementary map" with time index t, we will find coordinates $(x_m^{(t)}, y_n^{(t)})$ of the node where the maximum coherence values (maximums were taken with respect to all frequencies) attain maximal value with respect to all other nodes of the regular grid:

$$(x_m^{(t)}, y_n^{(t)}) = \arg\max_{(i,j)} \mu^{(t)}(x_i, y_j) \tag{10}$$

We will consider the nodes defined by (10) together for all three GPS components E, N and Up. The cloud of points with coordinates $(x_m^{(t)}, y_n^{(t)})$ which are regarded within some time interval $t \in [t_0, t_1]$ forms a rather random population.

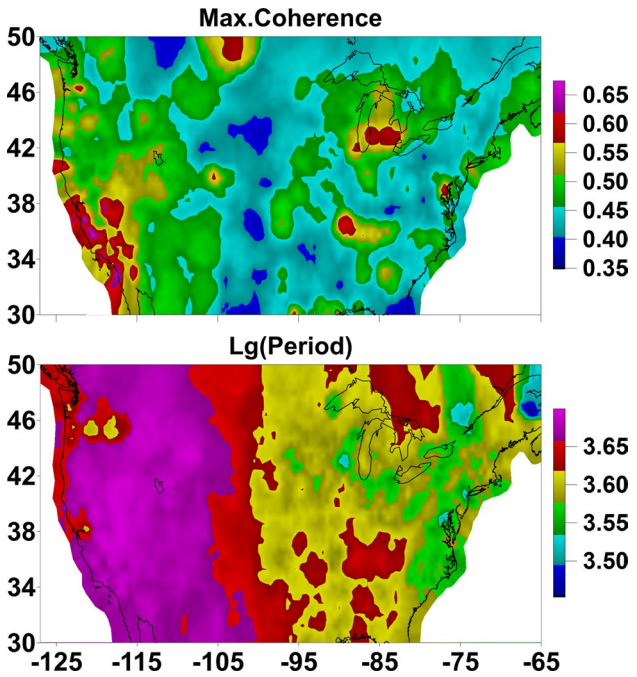

Fig. 4 Top map presents a weighted mean $\bar{\mu}_{ij}^{(WM)}$ of maximums of spectral coherence measures. The bottom map presents weighted mean $\bar{l}_{ij}^{(WM)}$ of averaged maps of decimal logarithms of periods (in minutes) corresponding to a maximum of multiple coherence

It is reasonable to estimate their 2D probability distribution function for each node (x_i, y_j) of the regular grid. For this purpose, we will use Parzen–Rosenblatt estimate with Gaussian kernel function (Duda et al. 2000):

$$p(x_i, y_j | t_0, t_1) = \sum_{t=t_0}^{t_1} \exp\left(-\frac{(x_i - x_m^{(t)})^2 + (y_j - y_n^{(t)})^2}{2h^2}\right) \Big/ \left(2\pi h^2 (t_1 - t_0 + 1)\right) \tag{11}$$

Here h is the radius of kernel averaging (smoothing bandwidth), t_0, t_1 are integers indexes which numerate "elementary" 5-day maps. Thus, $(t_1 - t_0 + 1)$ is the number of 5-day maps within the considered time interval. We used the smoothing bandwidth $h = 1°$. Figure 5 presents a map of probability density estimate (11) for all available time indexes t.

It is easy to notice a certain similarity between the "coherence spots" in Fig. 4 (left panel) and the areas of increased probability density in Fig. 5. However, there are significant differences. This is manifested by the fact that the correlation coefficient between grid vectors $\bar{\mu}_{ij}^{(WM)}$ and probability density defined by (11), for the whole history of observations is 0.5035 only. The 2-D probability density map provides information on where the maximum coherence values are most often achieved without taking into account the magnitudes of these maximum coherences. It seems that the use of probability densities provides a more informative picture of the spatial distribution of the features of the coherence field of earth tremors.

Some of the high-probability spots in Fig. 5 could easily be identified with different geological reasons. In particular, these are seismically active South California, Bakken oilfield, Denver area of induced seismicity (Hsien and Bredehoft 1981), and New Madrid seismicity zone.

If we take the moving time window $t \in [t_0, t_1]$ not over the whole history of observation but over some rather short time interval, then the sequence of plots which are similar to Fig. 5 will present a time-spatial dynamics of GPS noise field of coherence. In connection with this possibility, it is of interest to calculate some measure that would characterize the degree of diversity of the location of spots of high-probability density in space. As such a measure, it is natural to propose Shannon informational entropy (Gray 1990) of two-dimensional probability density:

$$En(t_0, t_1) = -\int_S p(x, y | t_0, t_1) \cdot \log(p(x, y | t_0, t_1)) \mathrm{d}x \mathrm{d}y / \log(|S|) \tag{12}$$

Here S is the 2D region under the investigation, and $|S|$ is its area. According to (12), the value of entropy is normalized $0 \le En \le 1$. For instance, for the map presented at Fig. 5 we have $En = 0.857$. Such high value of normalized entropy indicates that there are a lot of centers of probability concentration. Let us consider the sequence of time windows

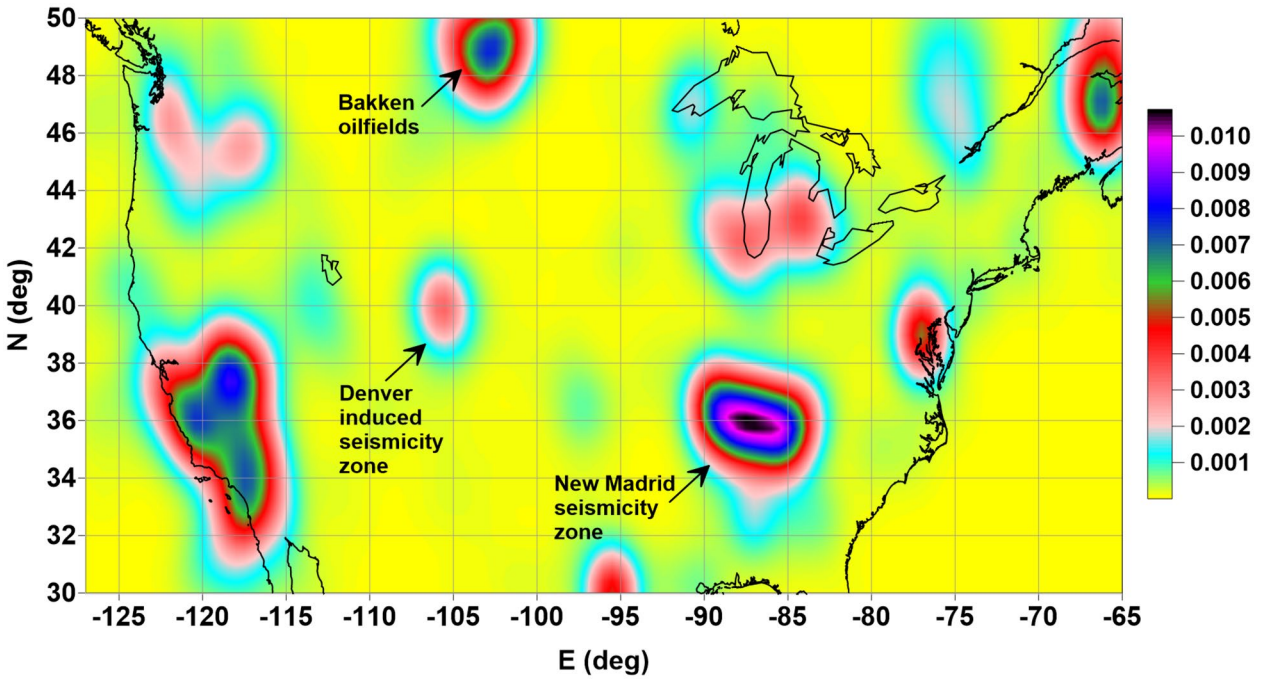

Fig. 5 Map of estimates the 2D probability density of the distribution of nodes of the regular grid, in which the maximum values of the maxima of the multiple spectral coherence function from the 10 nearest operational stations are reached. For each coherence function, the maximum value among the periods is taken, and for each time window 5 days long the node in which this maximum value reaches a maximum among all grid nodes is found. For each time window, grid nodes in which the maximum values of coherence are reached are searched simultaneously for all three components E, N and Up. The goal of constructing a map of 2D probability density is to highlight those areas in which maximum coherence values are most often achieved

of length 182 days (half year) taken with mutual shift of 14 days and estimate the entropy (12) of 2D density functions (11) for each time window. Figure 6 presents a graph of normalized entropy (12) for such sequence of time windows in dependence on the right-hand end of time windows.

Low entropy values at Fig. 6 correspond to a small number of local extremes of the two-dimensional density of the nodes where the maximum is reached, and large entropy values correspond to a large number of local maxima of the distribution density. The seasonal trend of entropy changes is noticeable: high values correspond to winter and low values to the summer season. In order to visually present the differences of maps of two-dimensional distribution densities for large and small entropy values, we calculate six such maps: three maps for small entropy values and three maps for large values. These maps are shown in Fig. 7.

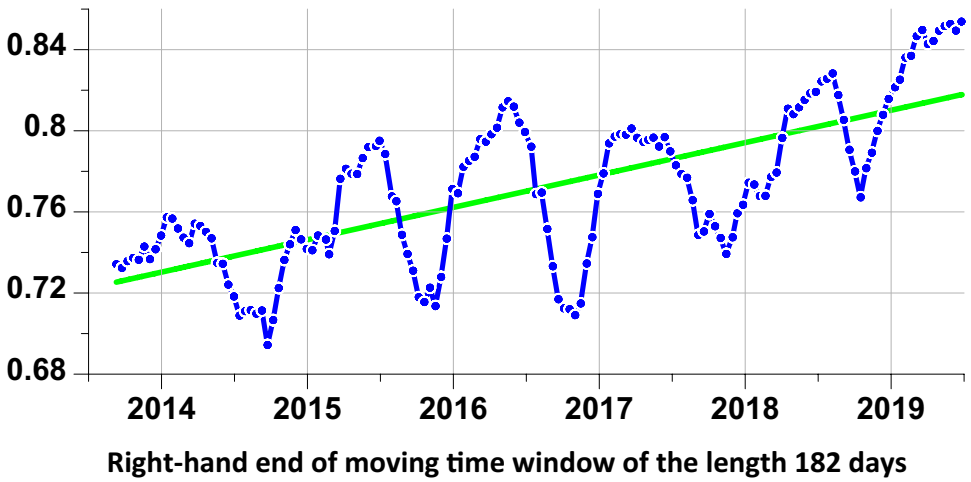

Fig. 6 Graph of the normalized entropy of 2D density functions within a length of 182 days, taken as mutual shift of 14 days for all three GPS components. The green line shows the general linear trend of entropy increasing. Graph is plotted in dependence on the right-hand end of moving time windows

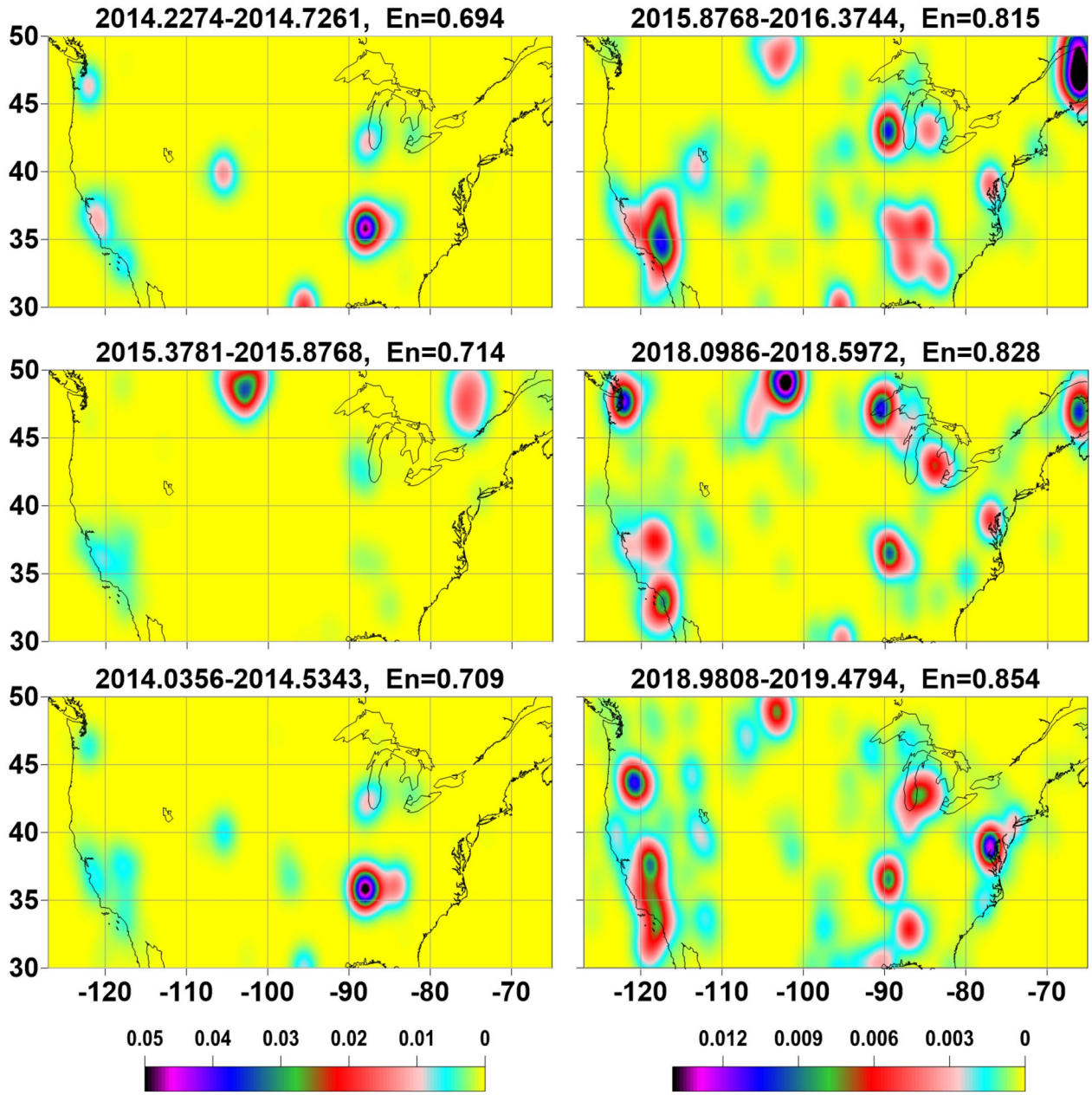

Fig. 7 Examples of 2D probability density functions corresponding to different time windows of the length 182 days. Left column presents examples of maps of 2D density distribution with "small" values of entropy, corresponding to three minimum local minima of the curve presented at Fig. 6. The right column presents examples with "large" values of entropy corresponding to three maximal local maxima of the curve presented at Fig. 6. The top of each panel shows the boundaries of time intervals measured in fractional years for which these maps were calculated and the values of normalized entropy. For instance, 2014.2274 means March 24, 2014, i.e., share of any year corresponds to the number of the day divided by the whole number of days within year. Maps in the left and right columns, respectively, have the same color scales which are placed below each panel

Figures 6 and 7 illustrate the fact that over the territory of the USA there is a seasonal periodicity in the properties of coherence of GPS noise, for which the maximum variety of places of concentration of the highest values of coherence falls on the winter period. This periodicity is superimposed on the general trend of increasing entropy, which is seen in Fig. 6.

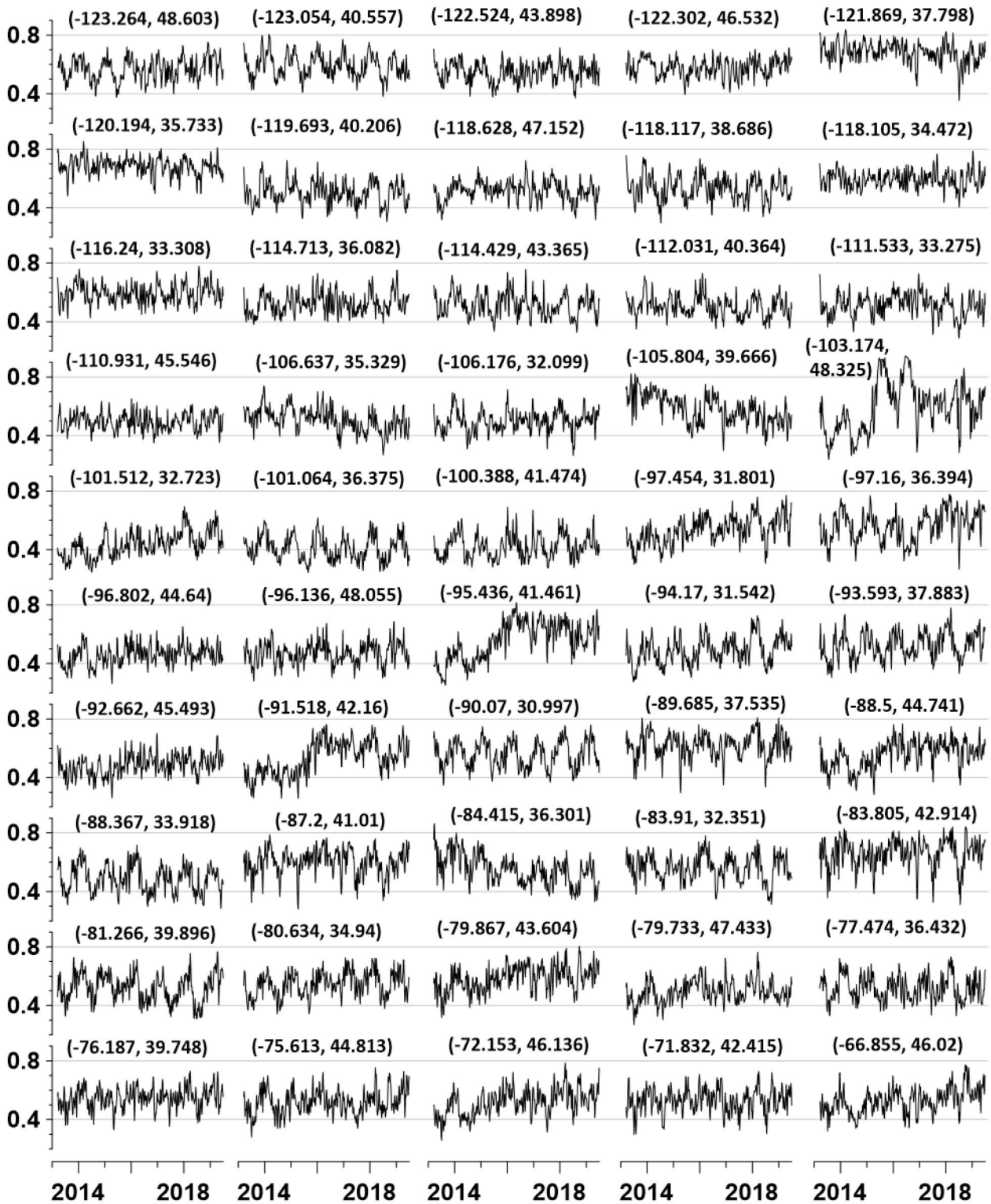

Fig. 8 Graphs of maximums of multiple coherence functions for the vertical component Up for 50 reference points, which were calculated from the 10 nearest operable GPS stations for the sequence of adjacent 5-day time windows. Geographical coordinates of the reference points (longitude, latitude) are put above each graph

Analysis of temporal dynamics using "secondary coherence"

Analyzing the temporal dynamics of the change in the GPS noise coherence field by computing averaged maps in sliding time windows, like the results presented in Fig. 7, is technically very difficult. Therefore, the idea arises to move from a detailed grid of nodes of size 50 by 125 to a coarser discrete model. Let us choose a certain number of reference points, more or less evenly covering the area under study. Figure 1 shows such a network of reference points, which are taken as centers of 50 clusters of GPS station positions. Next, we do the same procedure as for the nodes of the regular grid, that is, for each reference point we calculate the multiple spectral measures of coherence (2) from the 10 nearest operational stations in adjacent time windows of 5 days length. These 10 operational stations are mainly taken from the areas identified in Fig. 1 by the Voronoi polygons, which can be called the areas of influence of each reference point.

Figure 8 presents graphs of maximums of multiple spectral coherences estimated for 50 reference points in adjacent time windows of the length 5 days for the vertical GPS component Up. Thus, there is a 50-dimensional time series with sampling step 5 days. In each scalar component of this time series, there are 460 samples (more than 6 years of observations). Similar graphs could be plotted for horizontal GPS components E and N as well.

Many graphs in Fig. 8 show the presence of annual periodicity. If we calculate the average values for all 50 reference points, then the annual component will be underlined even more. Figure 9 shows the graphs of the average values for the reference points for all GPS components. It is noticeable that the average values, despite the pronounced seasonal component, are non-stationary. This suggests that some rhythms are possible, for which changes in the coherence measure at different reference points are more or less consistent (synchronous) with each other. Thus, the idea arises of calculating "coherence from coherences" or "secondary coherence."

To study the non-stationary effects of secondary coherence, we take a time window 180 days long or 36 samples with a time step of 5 days, for each of which we have 50 values of "primary maximum coherence" at the reference points. In each window with a length of 36 samples, we calculate all the pairwise modules of the coherence function using (6) and the fifth-order autoregression model for all different combinations of two-dimensional time series. With a total number of 50 time series, the number of such pairwise combinations is 1225. Further, we average the values of these pairwise coherence functions for all frequencies and as a result, we obtain the average measure of coherence in the sliding time window for a 50-dimensional time series. A similar procedure of using the mean of all by-pairs coherences with the help of the autoregression model for two-dimensional time series was applied in Lyubushin (2018b). Figure 10 shows time–frequency diagrams of such coherence measures separately for the three GPS components.

As can be seen from the time–frequency diagrams in Fig. 10, the secondary coherence of time series of the primary coherence at 50 reference points is highly non-stationary and at least two events can be distinguished, consisting in a sharp increase in secondary coherence in early 2016 and early 2018. These bursts of coherence arose mainly on periods from 18 to 28 days. In order to more accurately represent the time structure, it is possible to calculate in each time window the average values for all frequencies. These graphs of average values of secondary coherence are presented in Fig. 11. From Figs. 10 and 11, it can be seen that, in general, the properties of coherence for horizontal components are more synchronized than for vertical ones.

Conclusion

A new method for studying the coherence field of the earth tremors, based on the joint processing of a large number of three-dimensional GPS time series, is proposed. The method

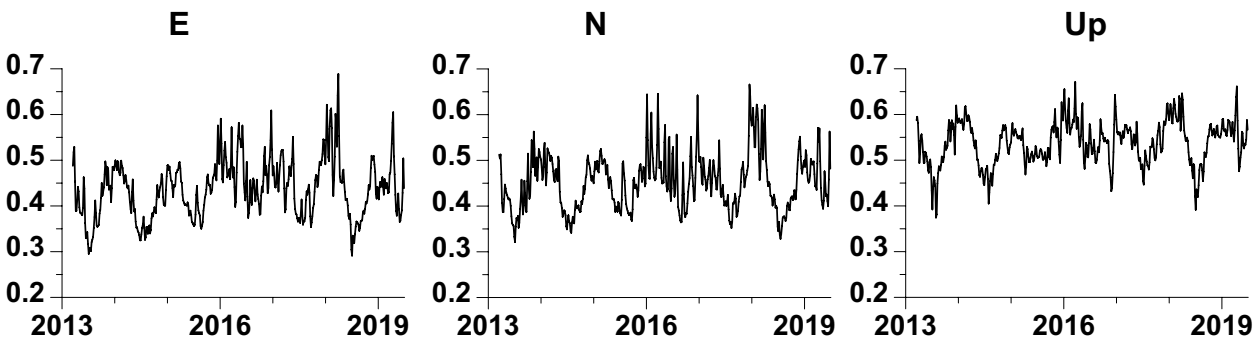

Fig. 9 Graphs of mean values of maximums of multiple coherence functions for 50 reference points from Fig. 8

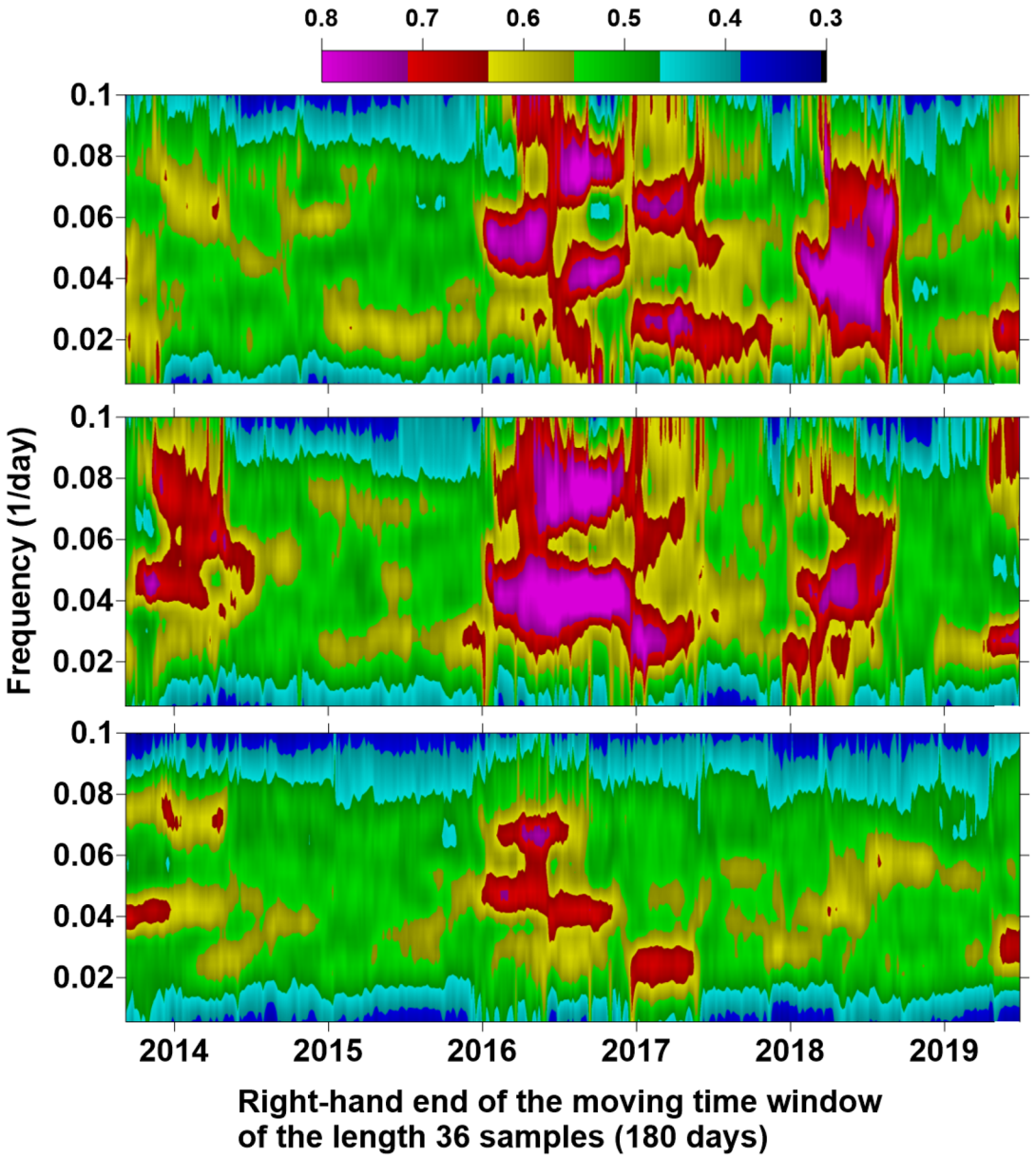

Fig. 10 Time–frequency diagrams for evolution of the mean of all by-pair coherences between values maximums of multiple coherence functions for 50 reference points for components E, N and Up ("secondary coherence"), estimated within moving time window of the length 36 samples (180 days). Diagrams are ordered from top to the bottom according to the sequence of E, N and Up GPS components and have the same color scale which is placed at the top of the figure

is based on the calculation of multiple spectral coherence functions in successive time windows of small length, tied to the nodes of the regular grid from a given number of the nearest operational stations. As a result of the data analysis, it is possible to construct averaged maps of the spatial distribution of the maximum of the multiple coherence function and the logarithm of the period at which the coherence maximum is reached, as well as the probability density of the distribution of those grid nodes in which the coherence maximum is most often achieved over space. The construction of these maps is possible using all the available data and also in a sliding time window, which makes it possible to trace the space–time dynamics of the coherence field of the earth tremors.

The method is illustrated with an example of analyzing GPS data with a time step of 5 min on a network covering the main US territory. Spots of increased coherence and increased probability density of nodes distribution, in which coherence maximum is most often realized, are identified. The positions of these spots coincide with areas

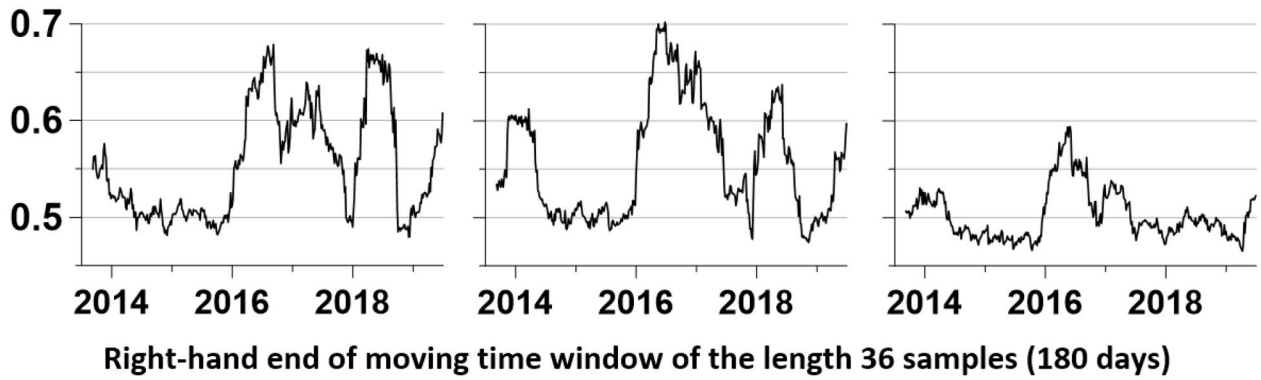

Fig. 11 Results of averaging over the frequencies of 2D time–frequency diagrams at Fig. 10. Averaging over the frequencies in each time window of the mean values of pairwise "secondary" coherences between the values of the "primary" coherences at 50 reference points for components E (left), N (middle) and Up (right)

of natural and induced seismicity, as well as with areas of shale gas production. The map of the logarithms of the periods at which the coherence maximum is realized clearly divides the territory of the USA into two parts with large and low values of the dominant coherence periods of approximately. The line of division is at about − 100° longitude. The cause of this division is presumably due to climatic differences between the western and eastern parts of the country. The use of entropy of two-dimensional probability densities allowed us to distinguish the seasonal rhythm of changes in the spatial properties of the coherence field. The summer period is characterized by a high concentration of points realizing the maximum coherence in space, and the winter period by a large variety of location of high-probability areas. The concept of "secondary coherence" is introduced as a measure of synchronization of variations of a multiple measures of coherence in a given number of reference points covering the area under study. As a result of constructing time–frequency diagrams of the variation of secondary coherence in a 180-day-long sliding window, a number of non-stationary effects were discovered—synchronization bursts between the primary coherence values at 50 reference points.

Acknowledgements The author is grateful to the Nevada Geodetic Laboratory, University of Nevada, Reno, for providing free access to three-component GPS time series with sampling time step 5 min from the global network all over the world. This work was supported by the Russian Foundation for Basic Research, Project No. 18-05-00133 "Estimation of fluctuations of seismic hazard on the basis of complex analysis of the Earth's ambient noise."

References

Beavan J (2005) Noise properties of continuous GPS data from concrete pillar geodetic monuments in New Zealand and comparison with data from US deep drilled braced monuments. J Geophys Res 110:B08410. https://doi.org/10.1029/2005JB003642

Blewitt G, Lavallee D (2002) Effects of annual signal on geodetic velocity. J Geophys Res 107(B7):2145. https://doi.org/10.1029/2001JB000570

Blewitt G, Hammond WC, Kreemer C (2018) Harnessing the GPS data explosion for interdisciplinary science. Eos 99. https://doi.org/10.1029/2018EO104623

Bock Y, Melgar D, Crowell BW (2011) Real-time strong-motion broadband displacements from collocated gps and accelerometers. Bull Seismol Soc Am 101(6):2904–2925. https://doi.org/10.1785/0120110007

Bos MS, Fernandes RMS, Williams SDP, Bastos L (2008) Fast error analysis of continuous GPS observations. J Geod 82(3):157–166. https://doi.org/10.1007/s00190-007-0165-x

Bos MS, Bastos L, Fernandes RMS (2010) The influence of seasonal signals on the estimation of the tectonic motion in short continuous GPS time-series. J Geodyn 49(3–4):205–209. https://doi.org/10.1016/j.jog.2009.10.005

Box GEP, Jenkins GM, Reinsel GC, Ljung GM (2015) Time series analysis—forecasting and control, 5th edn. Wiley, Hoboken

Brillinger DR (1975) Time Series. Data analysis and theory, holt, rinehart and winston, Inc, New York, Chicago, San Francisco.

Caporali A (2003) Average strain rate in the Italian crust inferred from a permanent GPS network—I: statistical analysis of the time-series of permanent GPS stations. Geophys J Int 155:241–253. https://doi.org/10.1046/j.1365-246X.2003.02034.x

Chen Q, van Dam T, Sneeuw N, Collilieux X, Weigelt M, Rebischung P (2013) Singular spectrum analysis for modeling seasonal signals from GPS time series. J Geodyn 72:25–35. https://doi.org/10.1016/j.jog.2013.05.005

Duda RO, Hart PE, Stork DG (2000) Pattern classification. Wiley, New York

Filatov DM, Lyubushin AA (2017) Fractal analysis of GPS time series for early detection of disastrous seismic events. Phys A 469(1):718–730. https://doi.org/10.1016/j.physa.2016.11.046

Filatov DM, Lyubushin AA (2019) Precursory analysis of GPS time series for seismic hazard assessment. Pure Appl Geophy First Online: January 7, 2019. https://doi.org/10.1007/s00024-018-2079-3

Goudarzi MA, Cocard M, Santerre R, Woldai T (2013) GPS interactive time series analysis software. GPS Solut 17(4):595–603. https://doi.org/10.1007/s10291-012-0296-2

Gray RM (1990) Entropy and information theory. Springer, New York

Hannan EJ (1970) Multiple time series. Wiley, New York
Hackl M, Malservisi R, Hugentobler U, Jiang Y (2013) Velocity covariance in the presence of anisotropic time correlated noise and transient events in GPS time series. J Geodyn 72:36–45. https://doi.org/10.1016/j.jog.2013.08.007
Hamilton JD (1994) Time series analysis. Princeton University Press, Princeton
Hsien PA, Bredehoft JD (1981) A reservoir analysis of the denver earthquakes: a case of induced seismicity. J Geophys Res 86(B2):903–920. https://doi.org/10.1029/JB086iB02p00903
Jolliffe IT (1986) Principal component analysis. Springer, Berlin
Khelif S, Kahlouche S, Belbachir MF (2013) Analysis of position time series of GPS-DORIS co-located stations. Int J Appl Earth Observ Geoinf 20:67–76. https://doi.org/10.1016/j.jag.2011.12.011
Langbein J (2008) Noise in GPS displacement measurements from Southern California and Southern Nevada. J Geophys Res 113:B05405. https://doi.org/10.1029/2007JB005247
Langbein J, Johnson H (1997) Correlated errors in geodetic time series, implications for time-dependent deformation. J Geophys Res 102(B1):591–603. https://doi.org/10.1029/96JB02945
Li J, Miyashita K, Kato T, Miyazaki S (2000) GPS time series modeling by autoregressive moving average method, application to the crustal deformation in central Japan. Earth Planets Space 52:155–162. https://doi.org/10.1186/BF03351624
Lyubushin AA (1998) Analysis of canonical coherences in the problems of geophysical monitoring. Izv Phys Solid Earth 34(1):52–58
Lyubushin AA (1999) Analysis of multidimensional geophysical monitoring time series for earthquake prediction. Ann Geofis 42(5):927–937. https://doi.org/10.4401/ag-3757
Lyubushin AA (2014) Analysis of coherence in global seismic noise for 1997–2012. Izv Phys Solid Earth 50(3):325–333. https://doi.org/10.1134/S1069351314030069
Lyubushin A (2018a) Synchronization of geophysical fields fluctuations. In: Chelidze T, Telesca L, Vallianatos F (eds) Complexity of seismic time series: measurement and applications. Elsevier, Amsterdam, pp 161–197
Lyubushin A (2018b) Global coherence of GPS-measured high-frequency surface tremor motions. GPS Solutions 22:116. https://doi.org/10.1007/s10291-018-0781-3
Mao A, Harrison CGA, Dixon TH (1999) Noise in GPS coordinate time series. J Geophys Res 104(B2):2797–2816. https://doi.org/10.1029/1998JB900033
Marple SL Jr (1987) Digital spectral analysis with applications. Prentice-Hall Inc, Englewood Cliffs
Teferle FN, Williams SDP, Kierulf HP, Bingley RM, Plag HP (2008) A continuous GPS coordinate time series analysis strategy for high-accuracy vertical land movements. Phys Chem Earth, Parts A/B/C 33(3–4):205–216. https://doi.org/10.1016/j.pce.2006.11.002
Wang W, Zhao B, Wang Q, Yang S (2012) Noise analysis of continuous GPS coordinate time series for CMONOC. Adv Space Res 49(5):943–956. https://doi.org/10.1016/j.asr.2011.11.032
Williams SDP, Bock Y, Fang P, Jamason P, Nikolaidis RM, Prawirodirdjo L, Miller M, Johnson DJ (2004) Error analysis of continuous GPS time series. J Geophys Res 109(B3):B03412. https://doi.org/10.1029/2003jb002741
Zhang J, Bock Y, Johnson H, Fang P, Williams S, Genrich J, Wdowinski S, Behr J (1997) Southern California permanent GPS geodetic array: Error analysis of daily position estimates and site velocities. J Geophys Res 102(B8):18,035–18,055. https://doi.org/10.1029/97JB01380

Alexey Lyubushin graduated from the Moscow Institute of Physics and Technology (1977). Ph.D. in numerical methods of optimal control in the Institute of Problems for Mechanics (1981). Doctor of sciences in mathematical methods of geophysical monitoring in the Institute of Physics of the Earth (1996). Since 1997 professor in Department of mathematics in the Russian State Geological Prospecting University.